





Influence factors on the seismic behavior and deformation modes of gravity retaining walls

ZHU Hong-wei^{1*}  <http://orcid.org/0000-0002-4740-8201>;  e-mail: zhw-1-zhw@163.com

YAO Ling-kan^{2,3}  <http://orcid.org/0000-0002-1933-5535>; e-mail: yaolk@home.swjtu.edu.cn

LI Jing¹  <http://orcid.org/0000-0002-4781-4074>; e-mail: yqssyzlj290@163.com

*Corresponding author

¹ School of Environment and Resource, Southwest University of Science and Technology, Mianyang 621010, China

² MOE Key Laboratory of High-speed Railway Engineering, Southwest Jiaotong University, Chengdu 610031, China

³ School of Civil Engineering, Southwest Jiaotong University, Chengdu 610031, China

Citation: Zhu HW, Yao LK, Li J, et al. (2019) Influence factors on the seismic behavior and deformation modes of gravity retaining walls. *Journal of Mountain Science* 16(1). <https://doi.org/10.1007/s11629-018-5009-z>

© Science Press, Institute of Mountain Hazards and Environment, CAS and Springer-Verlag GmbH Germany, part of Springer Nature 2019

Abstract: This study investigated the influence factors on the seismic response and deformation modes of retaining walls using large-scale model shaking table tests. Experimental results showed that the distribution of peak seismic earth pressures along the height of a wall was a single peak value curve. The seismic earth pressures on a gravel soil retaining wall were larger than the pressures on the weathered granite and quartz retaining walls. Also, the peak seismic earth pressure increased with increases in the peak ground acceleration and the wall height. The measured seismic active earth pressures on a rock foundation retaining wall were larger than the calculated values, and the action position of resultant seismic pressure was higher than 0.33 H. In the soil foundation retaining wall, the measured seismic earth pressures were much smaller than the calculated values, while the action position was slightly higher than 0.33 H. The soil foundation retaining wall suffered base sliding and overturning under earthquake conditions, while overturning was the main failure mode for the rock foundation retaining walls.

Keywords: Gravity retaining wall; Earthquake

Received: 13 May 2018

1st Revised: 29 July 2018

2nd Revised: 14 November 2018

Accepted: 20 December 2018

action; Seismic behavior; Deformation mode; Shaking table test

Introduction

Gravity retaining walls are used widely as retaining structures to support fill slopes adjacent to roads and residential areas. The May 12, 2008, Wenchuan earthquake, one of the largest recent seismic events in China, triggered numerous landslides and caused substantial damage to retaining walls as a result of earthquake-induced failures of fill slopes.

Studies investigating the effects of seismic activity on the deformation modes of gravity retaining walls have become an important topic in geotechnical engineering. The M-O method (Mononobe and Mastsuo 1929; Okabe 1924) has been proposed, which calculations seismic soil pressures on retaining structures. In recent years, a large number of scholars have focused on the prediction of seismic soil pressures, and many theoretical and model-based tests have been developed.

In the theoretical research, Veletsos and Younan (1997) proposed a new method to analyze

the stability of cantilever retaining walls. Their research revealed that for realistic wall flexibilities, the maximum wall forces are significantly lower than those obtained for fixed-based rigid walls and potentially of the same order of magnitude as those computed by the Mononobe-Okabe method. [Al Atik and Sitar \(2010\)](#) proposed a new pseudo-dynamic approach to calculate both active and passive seismic soil pressures on retaining walls by controlling mainly the pace value and acceleration value. [Gazetas et al. \(2004\)](#) treated backfill soil as a set of springs and considered the retaining wall as an ideal rigid plasticity body. He proposed a new pseudo-dynamic analysis method to calculate passive seismic earth pressures. Based on the Mononobe-Okabe method, [Green et al. \(2008\)](#) used a differential element analysis method and a differential equation to calculate the active pressure behind rigid retaining walls under earthquake conditions. They proposed interesting theoretical answers to explain the nonlinear distribution of the active pressures. In addition, [Kim et al. \(2013\)](#) developed improved methods for the calculation of seismic earth pressures that influence a gravity retaining wall by considering the cohesion between the soil and the wall. In addition, [Lee \(2014\)](#) presented an analytical solution to determine the seismic soil pressure distribution on a retaining wall with cohesive soils.

The seismic behavior of a retaining wall has been investigated experimentally using various methods, including soil element testing, centrifuge model testing ([Callisto et al. 2010](#)), and shake table testing at reduced ([Cattoni 2012](#); [Panah et al. 2015](#)) and at nearly full scale pressures ([Shahgholi et al. 2001](#); [Tatsuoka et al. 2009](#); [Wang et al. 2015](#)). [Whitman \(1990\)](#) conducted a centrifugal dynamic test of a cantilever retaining wall, and the results showed that the distribution of seismic active earth pressures along the retaining wall was nonlinear. [Yazdandoust \(2017a&b\)](#) carried out small-scale shake table tests on a 1-m-high rigid retaining wall model. He found that the distribution of seismic earth pressures along the wall had a parabola-like curve. According to the results of mechanical shake table tests, [Zhu et al. \(2012\)](#) found that the seismic earth pressures had a triangle-like distribution. The results show that the effect of seismic earth pressure of retaining walls depends mainly on the horizontal seismic acceleration while the effect of

vertical seismic acceleration is not significant.

Using large-scale shake table tests, [Zhang and Han \(2012\)](#) proposed a method to calculate the sliding displacement of a gravity retaining wall and also introduced the distribution of seismic earth pressures and their variation relationship with the displacement.

Overall, the common conclusion is that seismic earth pressures are distributed in a nonlinear manner along gravity retaining walls ([Bathurst and Hatami 1998](#); [Wang and Shi 1983](#); [Bergado et al. 1992](#)). The factors that affect the distribution and magnitude of seismic soil pressures on retaining walls, however, vary in magnitude and are complex. These factors depend on properties such as backfill soil, foundation types, peak ground accelerations (PGAs), wall height, and section patterns of the retaining wall as well as various other factors ([Anasua and Dilip 2016](#); [Roozbeh et al. 2016](#); [Pain et al. 2017](#)). Therefore, focusing narrowly on some factors and disregarding others would result in one-sidedness and prevent researchers from approaching the subject from a holistic perspective.

In this study, gravel soil, weathered granite, and quartz sand were selected as backfill material that was added to the soil in a retaining wall. Then we conducted a series of large-scale shake model tests on the model walls with both soil and rock foundations. First, we provided the background for the experimental design and explanation of the equipment and instrumentation used in this test. Then, an examination was conducted on the magnitude of the influence related to backfill properties, foundation types, earthquake magnitudes, and wall height on the response of gravity retaining walls to earthquake conditions.

1 Methods

A gravity retaining wall model was constructed and tested at the Key Laboratory of High Speed Railway Engineering facility located at Southwest Jiaotong University, Ministry of Education. A computer-controlled servo-hydraulic single degree of freedom (horizontal) shake table facility was used for seismic tests on the retaining wall model, and the shaking action was provided by a digitally controlled servo-hydraulic actuator. To The shaking table had a loading platform with

dimensions of 3.5 m × 1.5 m and a payload capacity of 2500 kg. The shake table operates within an acceleration range of 0.04–1.2 g with an amplitude of ±10 cm. A major limitation associated with model studies, especially in laboratory studies related to earthquake engineering, is the effect of the container boundary. The steel test box used for the tests was rectangular in cross-section with an inside dimension of 3.5 m × 1.5 m and 2.1 m deep. As recommended by [Bhattacharya et al. \(2012\)](#), to decrease the reflection of seismic waves and reduce the boundary friction, a 50 mm thick foam sheet was placed at the two lateral sides of the box, which can provide a low stiffness buffer between the wall and the backfill.

1.1 Physical model configuration and construction

A gravity retaining wall model was constructed of concrete with a trapezoid cross-section. The top and the bottom dimensions were 0.26 m and 0.68 m wide, respectively ([Figure 1](#)). The total height of the retaining wall model was 1.5 m, which was chosen per the capacity of the shaking table. In the test model, a concrete platform with a thickness of 0.15 m was used to simulate soil foundation, as shown in [Figure 2\(a\)](#). Besides, a boss was set in front edge of the concrete platform to simulate rock foundation, and the dimensions of the boss were 0.1m high and 0.2m wide ([Figure 2\(b\)](#)). The gravity retaining wall was placed on the concrete platform and they don't have rigid connection.

The retaining wall model was instrumented with acceleration transducers, seismic soil pressure sensors, and displacement transducers located at various locations. The analog voltage output acceleration transducers had full-scale acceleration ranges of 5 g along both the X- and Y-axes, with a bandwidth of 1–2 kHz. Strain-gauge seismic earth pressure sensors had a contact surface of 50 mm in diameter, a measuring capacity of 1000 kPa, and a sensitivity of 0.05 kPa. The sensing range of the displacement transducers was 2–40 mm, and their measuring error was less than 1%.

One accelerometer, A0, was installed to shake the table and record the base acceleration. The other six acceleration transducers (A1, A2, A3, A4, A5, and A6) were placed at elevations of 250 mm, 510 mm, 536 mm, 588 mm, and 602 mm,

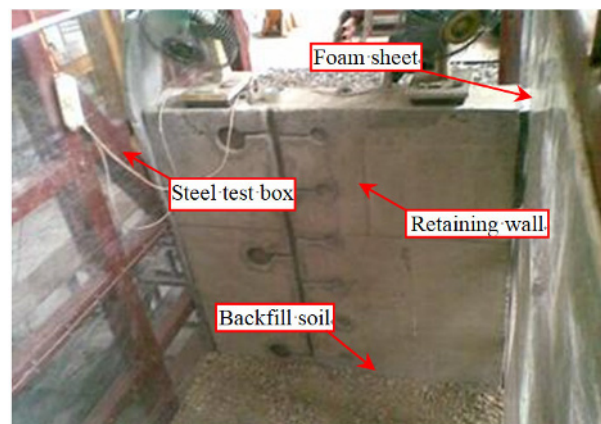


Figure 1 Construction of shaking table model of retaining wall.

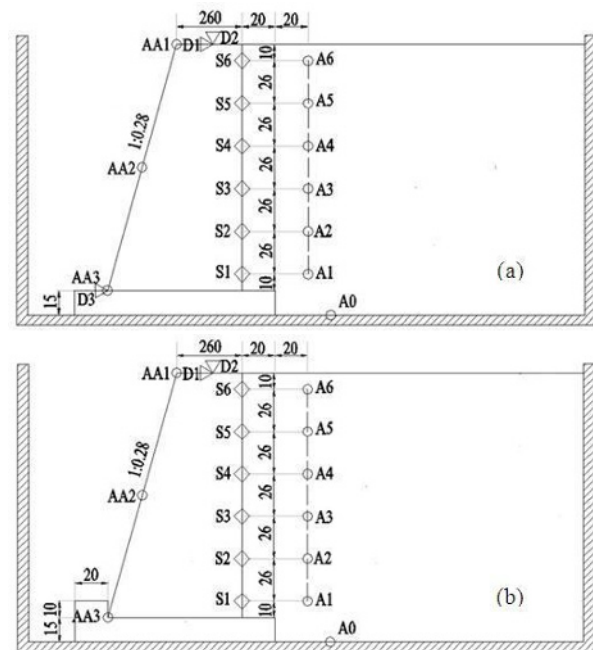


Figure 2 The sketch of the model, the rock foundation retaining wall (a) and the soil foundation retaining wall (b) (unit: cm).

respectively in the backfill. Six seismic soil pressure sensors (S1, S2, S3, S4, S5, and S6) were embedded at the same elevations along the central axis along the back of the retaining wall. To measure the horizontal displacement, two displacement transducers (D1 and D2) were positioned at the top and the bottom of the retaining wall. All sensors were connected to the 8-channel data acquisition system of the shake table, as illustrated in [Figure 2\(a\)](#) and [Figure 2 \(b\)](#).

Quartz sand, gravel soil, and weathered granite were used as backfill soils. Quartz sand properties are similar to that of weathered granite,

and according to a direct shear test, the internal friction angles were determined to be 37.4° and 34.5°, respectively, with apparent cohesions of 3.3 kPa and 4.1 kPa, respectively. Gravel soil is a common subgrade filling, and the internal friction angle was 42.3, with an apparent cohesion of 6.8kPa.

According to a grain size analysis test (Figure 3), the coefficient of curvature of quartz sand and weathered granite was the same, C_c was equal to 1.2, and the coefficient of uniformity, C_u , was 37.8 and 40.9, respectively. For gravel soil, the coefficient of curvature C_c was 1.3, and the coefficient of uniformity, C_u , was 6.8. To achieve uniform density, the backfill was dropped at the height of 0.5m so that the traveling speed of the soil could keep constant. In the model tests, the backfill soil was placed in layers, and the bulk unit weight of the backfill soil was maintained at 19.8 kN/m³, with a relative density, D_r , of 96%.

1.2 Similitude relationships of the model test

For the model wall tested in this study, the size of the wall was derived according to the density of the backfill soil and the payload capacity of the shake table. Therefore, the retaining wall model used in this study was constructed with a height of 1.5 m. Because soil behavior is nonlinear, the seismic response of the model may not truly reflect that of the prototype. As recommended by Jiang et al. (2009), using the prototype soil as backfill soil and keeping them have basically the same mass density and moisture content, that is to say, the dimensionless coefficient of the model backfill soil would be equal to the prototype soil.

To simulate 12 m, 8 m, and 4 m high prototype walls, the geometric similarity ratios were set at 8.0,

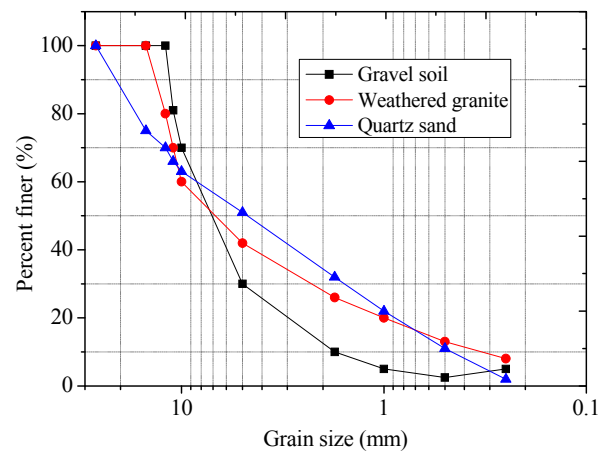


Figure 3 Grain-size distribution curves of backfill soils.

5.333, and 2.667, respectively. According to the laws of model similarity, in order to ensure the seismic characteristics of the model and prototype are similar, time duration of the input earthquake waves should be compressed. In the test model, time compression ratios were 4.76, 3.51, and 2.09, which simulated 12-m-, 8-m-, and 4-m-high prototype walls, respectively. The model dimension, density of backfill soil, acceleration, and time were selected to be the manipulated variables. The relationships of various physical quantities, such as length, density, acceleration, and others, were derived on the basis of the Buckingham π theorem. The primary similarity parameters are depicted in Table 1.

1.3 Seismic waves and the loading law

The shake table tests were conducted with an input of horizontal earthquake conditions. The seismic waves included a Da-rui synthetic wave, an El-Centro N-S wave (1940), and a Kobe N-S wave (1995), with maximum acceleration peak values of the input ground motion being 0.1 g, 0.2 g, and 0.4 g, respectively. These values corresponded to the probabilities of exceeding a 50-year event of 63%, 10%, and 2%. The predominant frequency of the seismic waves corresponded to 8 Hz, 5 Hz, and 2 Hz, respectively, which are well below the fundamental frequency of the retaining wall model (22 Hz). The code names of the seismic waves were DR, El, and KB, respectively. Figure 4 shows the Da-rui synthetic wave diagram and the Fourier amplitude spectrum.

Table 1 Primary similitude coefficients of the model.

Physical quantities	Similitude relationship	Similarity parameters		
		12 m	8 m	4 m
Length/ L	C_l	8.000	5.333	2.667
Density/ ρ	C_ρ	1	1	1
Acceleration/ a	C_a	1	1	1
Velocity/ v	$C_v=C_\rho^{1/4}C_l^{3/4}$	4.75	3.51	2.09
Displacement/ u	$C_u=C_\rho^{1/2}C_l^{3/2}$	22.63	12.32	4.36
Cohesion/ c	$C_c=C_\rho C_l$	8.00	5.33	2.67
Friction angel/ φ	$C_\varphi=1$	1	1	1
Time/ t	$C_t=C_\rho^{1/4}C_l^{3/4}$	4.75	3.51	2.09
Frequency/ ω	$C_\omega=C_\rho^{-1/4}C_l^{-3/4}$	0.210	0.285	0.479

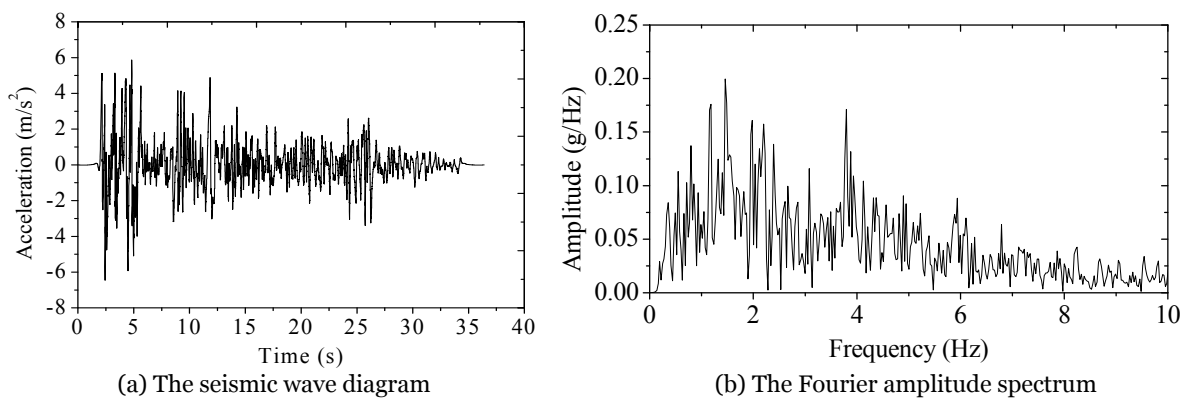


Figure 4 Compressed acceleration time-history curve of inputting seismic wave (Da-rui: X direction).

In order to observe and record the seismic characteristics of the retaining wall model, a white Gaussian noise with no less than 30 seconds was used to excite the model. The peak acceleration was approximately 0.03–0.05 g. The aim of the white Gaussian noise was to identify the frequency of the gravity retaining wall and the loading law of the shake table test, as shown in Table 2.

2 Results

2.1 Distribution of the peak seismic earth pressures

Figure 5 shows a time history record of the seismic earth pressures obtained from sensor S3 for the gravel soil retaining wall under the Da-rui

synthetic wave. According to the figure, the seismic earth pressure time history curve was consistent with the input seismic excitation. More succinctly, the seismic earth pressure increased (decreased) with an increase (decrease) in the input motion acceleration. As shown in Figure 5, the peak seismic earth pressure was 5.87 kPa.

Figure 6 shows the distribution of the peak seismic earth pressure along the height of the retaining wall on a rock foundation. The peak seismic earth pressure distribution was nonlinear along the height of the wall. Moreover, the observed data for the shaking table test observations for the model retaining wall under seismic condition measured by Zhang and Han (2012) had shown the non-linear variation of peak seismic active earth pressure along the depth of the wall, thus confirming the present findings. Figure 6(a) shows the distribution of the peak seismic earth pressure of different backfill soil retaining wall on a rock foundation at 0.4 g acceleration, it can be well observed that the backfill soil properties had a significant effect on the pressures. The mechanical properties of weathered granite were similar to quartz sand; both were homogenous mediums, and the strength and stiffness of weathered granite and quartz sand were lower than that of gravel soil and less compressible. For the rock foundation retaining wall, the dynamic action transferred directly to the back of the wall, likely because of the strong foundational restriction. Therefore, the peak seismic earth pressure distribution of the gravel soil

Table 2 The loading law of the shake table test.

Excitation sequence	Code	PGA/g	Compression ratio	Simulation height
1	WN-1	0.04	1	-
2, 3, 4	DR,EL,KB	0.1	4.75	12 m
5	WN-2	0.04	1	-
6, 7, 8	DR,EL,KB	0.1	3.51	8 m
9	WN-3	0.04	1	-
10, 11, 12	DR,EL,KB	0.1	2.09	4 m
13	WN-4	0.04	1	-
14, 15, 16	DR,EL,KB	0.2	4.75	12 m
17	WN-5	0.04	1	-
18, 19, 20	DR,EL,KB	0.2	3.51	8 m
21	WN-6	0.04	1	-
22, 23, 24	DR,EL,KB	0.2	2.09	4 m
25	WN-7	0.04	1	-
25, 26, 27	DR,EL,KB	0.4	4.75	12 m
28	WN-8	0.04	1	-
29, 30, 31	DR,EL,KB	0.4	3.51	8 m
32	WN-9	0.04	1	-
33, 34, 35	DR,EL,KB	0.4	2.09	4 m

retaining wall was larger than for the other two kinds of materials. Figure 6(b) shows the distribution of the peak seismic earth pressure of the gravel soil retaining wall on a rock foundation at 0.4 g acceleration, it can be seen that there was no significant difference in the peak seismic earth pressure distribution along the height of the retaining wall under the influence of the various earthquake waves. Figure 6(c) compares the distribution of the peak seismic earth pressure of the gravel soil retaining wall on a rock foundation under the Da-rui synthetic wave, it can be inferred that the peak seismic earth pressure distribution appeared to increase with increasing PGA. The results indicated that PGA was one of the main factors that affected the value and the distribution of the peak seismic earth pressure on the retaining wall, the results basically agree with the results in the literature (Yang et al. 2018).

Figure 6(d) shows the peak seismic earth pressures along the gravel soil retaining wall under the Da-rui synthetic wave with different heights at 0.4 g acceleration. It appeared that the peak seismic earth pressure not only was related to properties of the backfill soil and PGA but also to the height of the wall. The peak seismic earth pressure increased with the increasing height of the

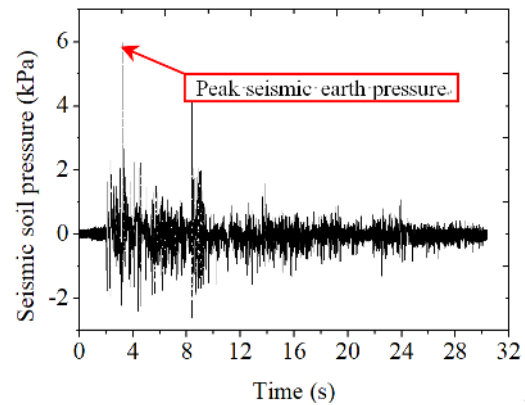


Figure 5 Dynamic soil pressure history of seismic soil pressure sensor (S3).

wall. As evidenced by the earthquake damage surveys of the Wenchuan earthquake region, it can be seen that the destruction rates of the higher retaining walls are larger than for lower ones in this extreme seismic area. The main cause of this phenomenon is that the natural frequency of the retaining wall decreases with an increase in wall height. Also, it appeared that the fundamental frequency of the retaining wall equaled that of the predominant seismic wave. Conversely, it appeared that it was easy for a retaining wall to experience coupled resonance destruction.

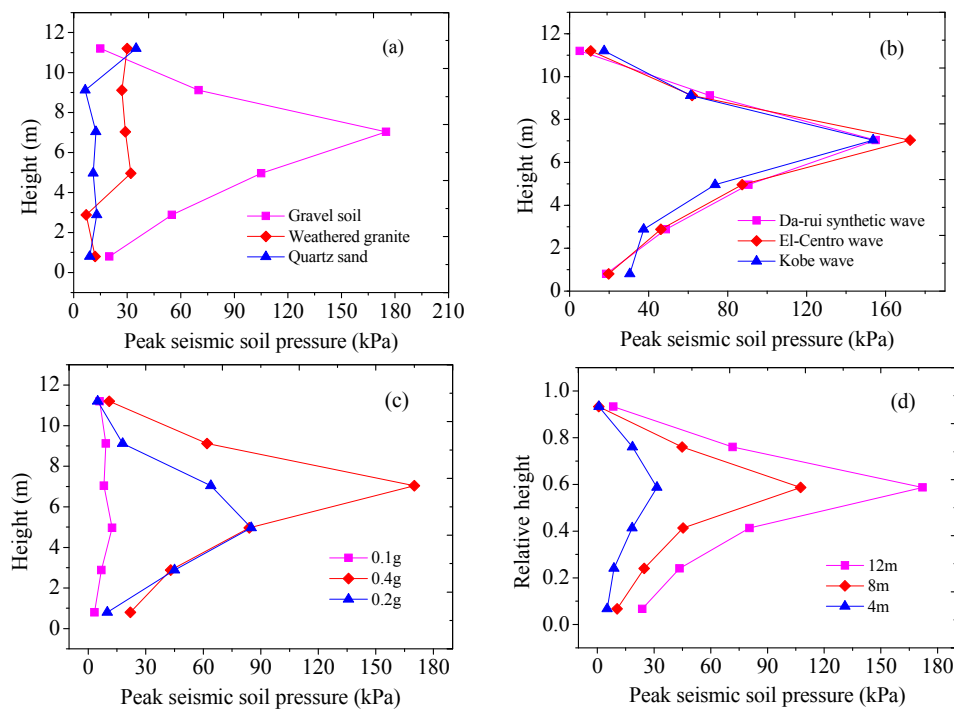


Figure 6 Distribution of peak seismic earth pressures under different backfill soils (a), different earthquake waves (b), different PGA (c), and different heights (d).

As a result of this analysis, it is concluded that the distribution curve of peak seismic earth pressures along the height of a retaining wall acted as a single peak value curve and that the maximum value was located approximately in the middle of the retaining wall height. Therefore, shear failure happens easily on stone retaining walls under earthquake conditions because of the existence of a joint. In addition, in the earthquake damage survey of retaining walls in the Wenchuan earthquake region, it was found that shear failure appeared primarily to stone retaining walls and even to concrete retaining walls (shown in Figure 7). Therefore, a calculation of the shear-resistant strength of a retaining wall in seismic design is necessary and important.

2.2 Comparison of measured values and calculated values of seismic active earth pressures

According to the pseudo-static seismic design approach (Mononobe-Okabe method), the seismic active earth pressure is computed as,

$$P_{AE} = \frac{1}{2} K_{AE} \mathcal{H}^2 \quad (1)$$

where K_{AE} is the seismic active earth pressure coefficient, is defined as,

$$K_{AE} = \frac{\cos^2(\varphi - \alpha)}{\cos^2 \alpha \left[1 + \sqrt{\frac{\sin \varphi \cdot \sin(\varphi - \alpha)}{\cos \alpha}} \right]^2} \quad (2)$$

where $\alpha = \tan^{-1} C_0$, φ and C_0 are the soil friction angle and seismic acceleration coefficient in horizontal directions.

Figure 8 shows the measured seismic active earth pressure values and the calculated values of the gravel soil retaining wall using Eqs. (1) and (2) at an acceleration amplitude of 0.2 g. In the case of the rock foundation retaining wall, the measured seismic active earth pressures were not different than the calculated values. For the soil foundation retaining wall, however, the measured values consistently underestimated the calculated values. An explanation for this difference is that the soil foundation retaining wall easily slipped under earthquake conditions. Hence, the seismic active earth pressure barely affected the back of the wall. Conversely, the rock foundation retaining wall



Figure 7 Shear failure of a stone retaining wall.

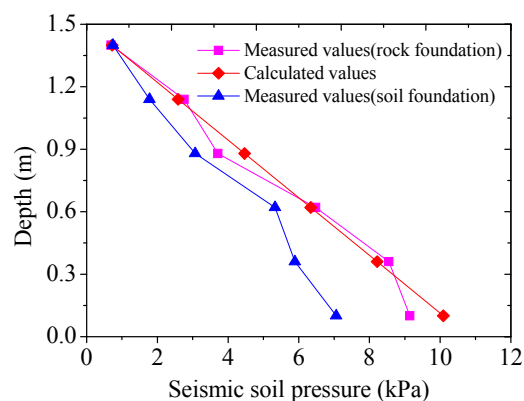


Figure 8 Seismic earth pressures for retaining walls with different foundation types.

suffered from a strong restriction because of the base, and hence the seismic response was more sensitive.

Table 3 lists the ratio of the resulting measured seismic earth pressure values to values calculated using the pseudo-static seismic design approach for a 12-m-high gravel soil retaining walls with different foundation conditions. The results show that the measured values were almost consistent with the calculated values of the rock foundation retaining wall at 0.1 g acceleration. As the PGA increased, however, the resulting measured seismic earth pressures were accordingly larger than the calculated values. For example, the resulting measured seismic active earth pressure was 1.24 times larger than the calculated values at 0.4 g acceleration. For the weathered granite and quartz sand retaining walls, however, the ratio of the resulting measured seismic earth pressures to the calculated values was slightly lower than 1.

In contrast, with an increase in PGA, the ratio of the resulting measured seismic earth pressures to the calculated values decreased for the gravel

soil retaining wall with a soil foundation. As noted earlier, this was a result of the fact that the soil foundation retaining wall could easily slip at the base at acceleration values of 0.2–0.4 g. The separation of the retaining wall from the soil resulted in very little seismic earth pressure influence on the back of the retaining wall. Therefore, the resulting measured seismic earth pressures were less than the calculated values for the soil foundation retaining wall. The measured values and the calculated values, however, were much closer for the weathered granite and quartz sand retaining walls.

Table 4 lists the action position of resultant seismic pressures to the 12-m-high retaining wall with different foundation conditions. It can be seen from the table that the action position is above a height of 0.33 H on the gravel soil retaining wall with the rock base, and the action position becomes higher with the increasing base excitation on the model wall. For instance, the action position was at a height of 0.34 H at an acceleration amplitude of 0.1 g, whereas at an acceleration amplitude of 0.4 g, the action position was at 0.41 H. Conversely, for the gravel soil retaining wall on the soil foundation, the action position was approximately at 0.33 H. For example, the action position was 0.34 H at 0.4 g acceleration, and there was no significant difference between the measured values and calculated values. The action position of resultant seismic pressure was slightly higher than the height of 0.33 H on the weathered granite and quartz sand retaining walls with a rock base. For instance, the action point was at 0.37 H on the weathered granite retaining wall at 0.4 g acceleration. For the weathered granite and quartz sand retaining walls on the soil base, the action positions were approximately 0.34 H and 0.35 H, respectively, and these heights were almost identical to the calculated values.

All these results indicated that the measured seismic active pressures always were larger than the calculated values, and the action positions of resultant seismic pressures were above a height of 0.33 H for the gravel soil retaining wall on the rock foundation. Therefore, overturning failure was the

Table 3 Ratio of the resulting measured seismic earth pressures to calculated values

Foundation type	Backfill	0.1 g	0.2 g	0.4 g
Rock foundation	Gravel soil	1.02	1.12	1.24
	Weathered granite	0.97	0.93	0.96
	Quartz sand	0.96	0.91	0.88
Soil foundation	Gravel soil	1.01	0.96	0.86
	Weathered granite	1.02	1.01	0.98
	Quartz sand	1.08	1.03	0.99

Table 4 Comparison of the action positions of resultant seismic pressures

Foundation type	Backfill	0.1 g	0.2 g	0.4 g
Rock foundation	Gravel soil	0.34	0.36	0.41
	Weathered granite	0.34	0.35	0.37
	Quartz sand	0.34	0.34	0.36
Soil foundation	Gravel soil	0.34	0.34	0.34
	Weathered granite	0.34	0.35	0.35
	Quartz sand	0.34	0.35	0.35

main failure mode for the retaining wall on a rock base, and the Mononobe-Okabe method was nonconservative in the design of the retaining wall on the rock foundation (i.e., danger for design). The resultant measured seismic pressures were smaller than the calculated values predicted using the pseudo-static seismic design approach for the soil foundation retaining wall. Also, the action positions of resultant pressures were slightly higher than 0.33 H, which had a small influence on the overturning moment in the soil foundation retaining wall. Therefore, the design of the soil foundation retaining wall according to the Mononobe-Okabe method still applied.

2.3 The deformation modes of the retaining walls under earthquake conditions

Figure 9(a) depicts the bottom and the top horizontal displacement under different base excitations in the quartz sand retaining wall with a soil foundation. It can be seen from the figure that there was no substantial deformation at the bottom at 0.1 g acceleration, and the top displacement was also very small, only about 1 mm. The retaining wall model deformed more at 0.2 g acceleration, and the horizontal displacement at the top and the bottom reached 19 mm and 14.7 mm, respectively. With an increase in PGA from 0.2 g to 0.4 g, the bottom displacement reduced to 10.2 mm, whereas the horizontal displacement at the top slightly increased. The final accumulative horizontal displacement was approximately 25.2 mm.

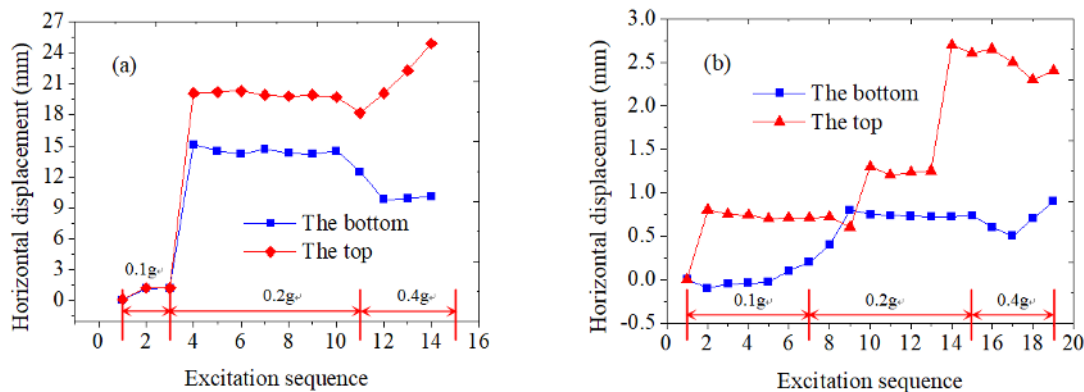


Figure 9 The deformation mode for the quartz retaining wall on a soil foundation (a) and the gravel retaining wall on a soil foundation (b).

Figure 9(b) shows the bottom and top horizontal displacements at different base excitations in the gravel soil retaining wall with a soil foundation. The figure shows that the horizontal displacement at the bottom was very small as a result of the action of small and moderate earthquakes (at 0.1 g and 0.2 g acceleration), and the top horizontal displacement was about 0.6 mm. However, there were large-scale displacements both at the bottom and the top of the retaining wall at 0.4 g acceleration. The displacement at the top and at the bottom reached 2.6 mm and 0.7 mm, respectively. Note that the soil foundation retaining wall suffered not only base sliding but also overturning under the higher seismic loads.

In addition, it will be also observed that the retaining wall experiences a process with the increase of earthquake acceleration, from an initial active state to a full active state, according to Dubrova’s study (Dubrova et al. 2013), between these two extremes, intermediate active states exist. The initial active state refers to a stage when only the retaining wall experiences a little displacement. The full active state occurs when the retaining wall experiences a large displacement. At intermediate active state, the displacement has little change or increases slowly. Take the gravel retaining wall on a soil foundation as example, when the acceleration less than 0.2g, the retaining wall was in an initial active state, when the acceleration less than 0.4g and large than 0.2g, the retaining wall transformed from an initial active state to an intermediate active state, when the acceleration larger than 0.4g, the retaining wall was in an full active state.

Moreover, Figure 9 also indicates that

overturning was the predominant mode for the gravel soil and quartz sand retaining walls on soil foundations at 0.1 g acceleration. With an increase in the PGA, the failure mode transformed from overturning to a combined mode (overturning and base sliding), and the horizontal displacement of the gravel soil retaining wall was smaller than that of the quartz sand retaining wall. The main reason for this was that gravel soil has high strength, good stability, and easy compaction. In addition, an increase in the degree of compaction of the backfill soil favored a decrease in the displacement of the retaining wall during an earthquake.

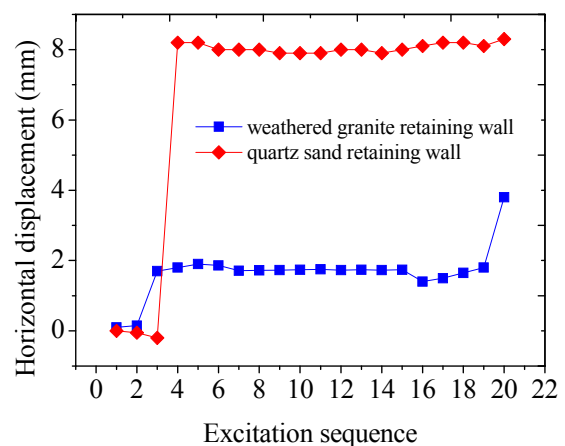


Figure 10 Deformations of the weathered granite and quartz sand retaining walls on rock foundations.

Figure 10 shows the horizontal displacement of the top of weathered granite and quartz sand retaining walls with rock foundations. Because of the constraint of the foundation, the retaining wall experienced very little displacement at the bottom. This figure shows that the horizontal displacement at 0.1 g acceleration was no different than at 0.2 g

acceleration, which was approximately 1.7–1.8 mm. Moreover, the top horizontal displacement decreased at 0.4 g acceleration, reducing to 1.1 mm. After that, the top horizontal displacement increased quickly, and the final accumulative displacement was approximately 3.6 mm. For the quartz sand retaining wall, there was almost no displacement at 0.1 g acceleration, while the displacement increased to 8.1 mm at acceleration amplitude of 0.2 g. The horizontal displacement remained approximately steady after that, but the displacement increased slightly until 0.4 g acceleration, and finally reached 8.3 mm after loading.

The authors hypothesize in this study that the soil foundation retaining wall suffered not only base sliding, but also overturning, whereas in the rock foundation retaining wall, overturning was the predominant failure mode. The test phenomenon was consistent with the results of earthquake damage investigations (shown in Figure 11). Furthermore, the characteristics of backfill soil had a large influence on the deformation mode of the gravity retaining wall. Under the same foundation condition, although the deformation modes of the differently backfilled retaining walls were the same, the horizontal displacement was significantly different. For instance, the accumulated displacement of the weathered granite retaining wall was 56.6% less than that of the quartz sand retaining wall on the rock foundation. Also, the difference in the displacement between the gravel soil retaining wall and the quartz sand retaining wall was even greater with a soil foundation.

3 Conclusions

(1) The distribution of peak dynamic soil pressures along the height of a gravity retaining wall was in the form of a single peak value curve, and the peak dynamic soil pressure was mainly related to PGA, wall height, and backfill properties. Moreover, peak dynamic earth pressures increased with an increase in the wall height and the PGA, but the effect of different earthquake wave frequencies on the peak dynamic earth pressures



Figure 11 Deformation modes of retaining walls on soil foundation (a) and rock foundation (b).

was small.

(2) Measured seismic active earth pressures were always larger than calculated values, and the action positions of resultant pressures were higher than the wall height, specifically 0.33 times higher in retaining walls with rock foundations. Measured resultant seismic pressures were all less than the values calculated using the pseudo-static seismic design approach for soil foundation retaining walls, and the action position of resultant pressures was slightly higher than 0.33 H. Therefore, it is necessary to evaluate the anti-overturning capacity of a rock foundation retaining wall. In soil foundation retaining walls, attention should be paid to their anti-sliding stability.

(3) Overturning was the main failure mode for rock foundation retaining walls as a result of the constraint of their foundations. Base sliding, however, was the main failure mode for soil foundation retaining walls. Moreover, the horizontal displacements of retaining walls with the same foundation conditions were very different with different backfill soils. The final accumulative displacement of seismic soil pressures in the gravel soil retaining wall on a soil foundation was significantly smaller than the displacement of the weathered granite and quartz retaining walls.

Acknowledgements

This research was funded by the National Program on Key Research Project of China (Grant No. 2016YFC0802206), the open research fund of MOE Key Laboratory of High-speed Railway Engineering,

Southwest Jiaotong University and Doctoral Innovation Fund Program of Southwest University of

Science and Technology (Grant No. 16zx7123).

References

- Al Atik L, Sitar N (2010) Seismic earth pressures on cantilever retaining structures. *Journal of Geotechnical and Geoenvironmental Engineering* 136(10): 1324-1333. [https://doi.org/10.1061/\(ASCE\)GT.1943-5606.0000351](https://doi.org/10.1061/(ASCE)GT.1943-5606.0000351)
- Anasua G, Dilip KB (2016) Reliability coupled sensitivity-based seismic analysis of gravity retaining wall using pseudostatic approach. *Journal of Geotechnical & Geoenvironmental Engineering* 142(6): 325-336. [https://doi.org/10.1061/\(ASCE\)GT.1943-5606.0001467](https://doi.org/10.1061/(ASCE)GT.1943-5606.0001467)
- Bathurst RJ, Hatami K (1998) Seismic response analysis of a geosynthetic-reinforced soil retaining wall. *Geosynthetics International* 5(1-2): 127-166. <https://doi.org/10.1680/gein.5.0117>
- Bergado DT, Lo KH, Chai JC (1992) Pullout tests using steel grid reinforcements with low-quality backfill. *Journal of Geotechnical Engineering* 118(7): 1047-1062. [https://doi.org/10.1061/\(ASCE\)0733-9410\(1992\)118:7\(1047\)](https://doi.org/10.1061/(ASCE)0733-9410(1992)118:7(1047))
- Bhattacharya S, Lombardi D, Dihoru L (2012) Model container design for soil-structure interaction studies. In: *Role of Seismic Testing Facilities in Performance-Based Earthquake Engineering*. Springer, Dordrecht, pp 135-158. https://doi.org/10.1007/978-94-007-1977-4_8
- Callisto L, Soccodato FM (2010) Seismic design of flexible cantilevered retaining walls. *Journal of Geotechnical and Geoenvironmental Engineering ASCE* 136(2): 344-354. [https://doi.org/10.1061/\(ASCE\)GT.1943-5606.0000216](https://doi.org/10.1061/(ASCE)GT.1943-5606.0000216)
- Cattoni E, Cecconi M, Pane V, et al. (2012) Development of DDBD method for retaining walls subjected to seismic loads. In: *International conference on performance-based design in earthquake geotechnical engineering*, Taormina, Italy, pp 1510-1521.
- Dubrova GA (2013) Interaction between soils and structures. *Rechnoi Transport* 42(3): 40-45. (In Russian)
- Gazetas G, Psarropoulos PN, Anastasopoulos I, Gerolymos N (2004) Seismic behaviour of flexible retaining systems subjected to short-duration moderately strong excitation. *Soil Dynamics and Earthquake Engineering* 24(7): 537-550. <https://doi.org/10.1016/j.soildyn.2004.02.005>
- Green RA, Olgun CG, Cameron WI (2008) Response and modeling of cantilever retaining walls subjected to seismic motions. *Computer-Aided Civil and Infrastructure Engineering* 23(4): 309-322. <https://doi.org/10.1111/j.1467-8667.2007.00538.x>
- Jiang LW, Yao LK, Wang J (2009) Similitude for shaking table model test on side slope relating to dynamic characteristics and strength. *Journal of Transport Science and Engineering* 25(2): 1-7. (In Chinese)
- Kim DS, Lee SH, Choo YW, Perdrat J (2013) Self-balanced earthquake simulator on centrifuge and dynamic performance verification. *KSCE Journal of Civil Engineering* 17(4): 651-661. <https://doi.org/10.1007/s12205-013-1591-3>
- Lee SH, Choo YW, Kim DS (2013) Performance of an equivalent shear beam (ESB) model container for dynamic geotechnical centrifuge tests. *Soil Dynamics and Earthquake Engineering* 44: 102-114.
- Mononobe N, Matsuo H (1929) On the determination of earth pressure during earthquakes. *Proc. World engineering congress, Tokyo, Vol. 9*, p. 388.
- Okabe S (1924) General theory of earth pressures and seismic stability of retaining wall and dam. *J Japanese Society of Civil Engineers, Vol 12, No. 1*.
- Pain A, Choudhury D, Bhattacharyya SK (2017) Effect of dynamic soil properties and frequency content of harmonic excitation on the internal stability of reinforced soil retaining structure. *Geotextiles and Geomembranes* 45(5): 471-486. <https://doi.org/10.1016/j.geotexmem.2017.07.003>
- Panah AK, Yazdi M, Ghalandarzadeh A (2015) Shaking table tests on soil retaining walls reinforced by polymeric strips. *Geotextiles and Geomembranes* 43(2): 148-161. <https://doi.org/10.1016/j.geotexmem.2015.01.001>
- Roosbeh GM, Gabriel C, Nicholas S (2016) Seismic earth pressures on retaining structures and basement walls in cohesionless soils. *Journal of Geotechnical & Geoenvironmental Engineering* 142(10): 415-423. [https://doi.org/10.1061/\(ASCE\)GT.1943-5606.0001507](https://doi.org/10.1061/(ASCE)GT.1943-5606.0001507)
- Shahgholi M, Fakher A, Jones CJFP (2001) Horizontal slice method of analysis. *Geotechnique* 51(10): 881-885. <https://doi.org/10.1680/geot.51.10.881.41058>
- Tatsuoka F, Munoz H, Kuroda T (2012) Stability of existing bridges improved by structural integration and nailing. *Soils and Foundations* 52(3): 430-448. <https://doi.org/10.1016/j.sandf.2012.05.004>
- Veletsos AS, Younan AH (1997) Dynamic response of cantilever retaining walls. *Journal of Geotechnical and Geoenvironmental Engineering* 123(2): 161-172. [https://doi.org/10.1061/\(ASCE\)1090-0241\(1997\)123:2\(161\)](https://doi.org/10.1061/(ASCE)1090-0241(1997)123:2(161))
- Wang L, Chen G, Chen S (2015) Experimental study on seismic response of geogrid reinforced rigid retaining walls with saturated backfill sand. *Geotextiles and Geomembranes* 43(1):35-45. <https://doi.org/10.1016/j.geotexmem.2014.11.006>
- Wang YQ, Shi SY (1983) Nonlinear distribution of earth pressure during earthquake. *Journal of Hohai University* 4(1): 61-72. (In Chinese)
- Whitman RV (1990) Seismic design behaviour of gravity retaining walls. In: *Proceedings of ASCE specialty conference on design and performance of earth retaining structures*. ASCE Geotechnical Specialty Publication, New York, 25 pp 817-842
- Yang CW, Zhang JJ, Wang ZZ, et al. (2018) Research on time-frequency analysis method of active earth pressure of rigid retaining wall subjected to earthquake. *Environmental Earth Sciences* 77: 232. <https://doi.org/10.1007/s12665-018-7325-6>
- Yazdandoust M (2017a) Investigation on the seismic performance of steel-strip reinforced-soil retaining walls using shaking table test. *Soil Dynamics and Earthquake Engineering* 97: 216-232. <https://doi.org/10.1016/j.soildyn.2017.03.011>
- Yazdandoust M (2017b) Experimental study on seismic response of soil-nailed walls with permanent facing. *Soil Dynamics & Earthquake Engineering* 98: 101-119. <https://doi.org/10.1016/j.soildyn.2017.04.009>
- Zhang JJ, Han PF (2012) Displacement based seismic design method for gravity retaining walls-Large scale shaking table tests. *Chinese Journal of Geotechnical Engineering* 34(3): 417-423. (In Chinese)
- Zhu HW, Yao LK, Liu ZS (2012) Comparison of dynamic characteristics between netted and packaged reinforced soil retaining walls and recommendations for seismic design. *Chinese Journal of Geotechnical Engineering* 34(11): 2072-2080. (In Chinese)